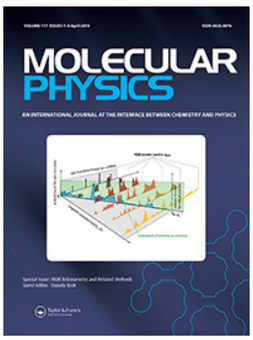

Taylor & Francis
Taylor & Francis Group

Molecular Physics

An International Journal at the Interface Between Chemistry and Physics

ISSN: 0026-8976 (Print) 1362-3028 (Online) Journal homepage: https://www.tandfonline.com/loi/tmph20

Aspects of structural order in ^{209}Bi-containing particles for potential MRI contrast agents based on quadrupole enhanced relaxation

Hermann Scharfetter, Christian Gösweiner, Paul Josef Krassnig, Carina Sampl, Martin Thonhofer, Roland Fischer, Stefan Spirk, Rupert Kargl, Karin Stana-Kleinschek, Evrim Umut & Danuta Kruk

To cite this article: Hermann Scharfetter, Christian Gösweiner, Paul Josef Krassnig, Carina Sampl, Martin Thonhofer, Roland Fischer, Stefan Spirk, Rupert Kargl, Karin Stana-Kleinschek, Evrim Umut & Danuta Kruk (2019) Aspects of structural order in ^{209}Bi-containing particles for potential MRI contrast agents based on quadrupole enhanced relaxation, Molecular Physics, 117:7-8, 935-943, DOI: 10.1080/00268976.2018.1511869

To link to this article: https://doi.org/10.1080/00268976.2018.1511869

Published online: 22 Aug 2018.

MOLECULAR PHYSICS
2019, VOL. 117, NOS. 7–8, 935–943
https://doi.org/10.1080/00268976.2018.1511869

Taylor & Francis
Taylor & Francis Group

NMR RELAXOMETRY AND RELATED METHODS

Aspects of structural order in ^{209}Bi-containing particles for potential MRI contrast agents based on quadrupole enhanced relaxation

Hermann Scharfetter[a], Christian Gösweiner[a], Paul Josef Krassnig[a], Carina Sampl[b], Martin Thonhofer[c], Roland Fischer[d], Stefan Spirk[b], Rupert Kargl[c], Karin Stana-Kleinschek[c], Evrim Umut[e] and Danuta Kruk[e]

[a]Institute of Medical Engineering, Graz University of Technology, Graz, Austria; [b]Institute of Paper, Pulp and Fiber Technology and Institute for Chemistry and Technology of Materials, Graz University of Technology, Graz, Austria; [c]Laboratory for Characterization and Processing of Polymers (LCPP), Faculty of Mechanical Engineering, University of Maribor, Maribor, Slovenia; [d]Institute of Inorganic Chemistry Graz University of Technology, Graz, Austria; [e]Faculty of Mathematics and Computer Science, University of Warmia and Mazury in Olsztyn, Olsztyn, Poland

ABSTRACT

Quadrupole relaxation enhancement (QRE) has been suggested as the key mechanism for a novel class of field-selective, potentially responsive magnetic resonance imaging contrast agents. In previous publications, QRE has been confirmed for solid compounds containing ^{209}Bi as the quadrupolar nucleus (QN). For QRE to be effective in aqueous dispersions, several conditions must be met, i.e. high transition probability of the QN at the ^{1}H Larmor frequency, water exchange with the bulk and comparatively slow motion of the Bi-carrying particles. In this paper, the potential influence of structural order within the compounds ('crystallinity') on QRE was studied by nuclear quadrupole resonance (NQR) spectroscopy in one crystalline and two amorphous preparations of Triphenylbismuth ($BiPh_3$). The amorphous preparations comprised (1) a shock-frozen melt and (2) a granulate of polystyrene which contained homogeneously distributed $BiPh_3$ after common dissolution in THF and subsequent evaporation of the solvent. In contrast to the crystalline powder which exhibits strong, narrow NQR peaks the amorphous preparations did not reveal any NQR signals above the noise floor. From these findings, we conclude that the amorphous state leads to a significant spectral peak broadening and that for efficient QRE in potential contrast agents structures with a high degree of order (near crystalline) are required.

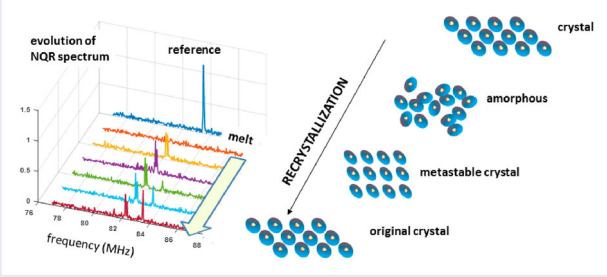

ARTICLE HISTORY
Received 30 June 2018
Accepted 3 August 2018

KEYWORDS
Quadrupole enhanced relaxation; magnetic resonance imaging; nuclear quadrupole resonance; triphenylbismuth; recrystallisation

Introduction

Recently, it was suggested to apply quadrupolar relaxation enhancement (QRE) as the central mechanism for a new class of extrinsic magnetic resonance imaging (MRI) contrast agents which rely on the shortening of the T_1 relaxation time constant of water protons [1,2]. QRE effects stem from the fact that protons can transfer their magnetisation to a quadrupolar nucleus (QN, i.e. a nucleus with spin quantum number ≥ 1) via a mutual, dipole–dipole (DD) coupling. This process can only occur at magnetic fields at which the proton resonance frequency matches one of the transition frequencies of the QN between its energy levels. It manifests itself as a fast decay of the proton magnetisation interpreted as an enhanced spin–lattice relaxation rate $R_1 = 1/T_1$ [1–8] referred to as quadrupole peaks. The position of the

CONTACT Hermann Scharfetter hermann.scharfetter@tugraz.at Institute of Medical Engineering, Graz University of Technology, Stremayrgasse 16, 8010 Graz, Austria

Supplemental data for this article can be accessed here. https://doi.org/10.1080/00268976.2018.1511869

quadrupole peaks is a function of the static magnetic field B_0, the electric field gradient (EFG) at the location of the nucleus, the electrical quadrupole moment of the QN, its spin quantum number I and the angle Θ between EFG and B_0 [1–11].

The most special feature is that, in contrast to typical paramagnetic MRI contrast agents, [12–16] QRE leads to narrow peaks and steep slopes [1,2,4,5,8–11]. In fact, such QRE peaks were observed for ^{14}N in the amide groups of proteins [17–19] and used for the first time for MRI contrast at very low B_0 [20] in humans. Despite these findings QRE has not yet been considered for extrinsic MRI contrast agents. However, from the above conditions it becomes clear that QRE can be controlled both by B_0 as well as by changing the chemical environment of the QN, i.e. by deformations of the electronic cloud close to the QN. This multiple dependences open the door for building responsive probes for molecular and theranostic imaging by MRI at typical clinical or pre-clinical field strengths between 1.5 and 7 T. QRE compounds could thus lead to highly field-selective biomarkers with a significant change in relaxivity upon activation in response to physiological alterations such as temperature, metal ions, redox state, enzyme activity or pH. The sensitivity to B_0 allows for switching on and off the contrast from the MRI device in case that the static field can be modulated somewhat, which is also a desirable feature because it allows for background subtraction and artefact detection in an easily repetitive manner. In this paper, we focus on compounds containing ^{209}Bi and on a B_0 of 3 T, i.e. a f_L of 123–128 MHz, depending on the exact B_0 values of the individual commercially available scanners.

There are several reasons for selecting Bismuth as a promising nucleus for QRE, as has also been detailed in [1]: (1) as QRE scales with the spin quantum number, Bi ($I = 9/2$) is favourable, (2) there exist many Bi-compounds with quadrupolar transition frequencies close to those needed for clinical field strengths, i.e. 1.5 and 3 T, (3) derivates of Bi-Aryl compounds can be synthetised in a fairly flexible manner and there exist many stable compounds, and (4) the toxicity potential of several Bi-Aryl compounds with stable Bi–C–bonds is expected to be low as has been reported in [21] and also dextran-coated Bi-iron-oxide nanohybrid particles have been reported to be fairly bio-compatible up to 1.6 mmol/kg body weight in mice [22].

Figure 1 shows an example of QRE effects observed for solid tris(2-oxymethyl-phenyl)bismuthane acquired with the experimental protocol described in [2]. One can clearly see the above-mentioned sharp peaks in ^{1}H spin–lattice relaxation rates at specific field strengths.

Though experimental NMRD data of ^{209}Bi-compounds have only been published for solids so far, quantum-mechanical models for simulating QRE of freely rotating ^{1}H–^{209}Bi systems strongly indicate the existence of pronounced QRE peaks also in liquid states. The theory behind this mechanism relies on a stochastic Liouville formalism and is not in the scope of this paper. For the interested reader, a comprehensive introduction can be found in [3–5,10].

For efficient QRE in particular scanners the following conditions have to be fulfilled:

(1) As the magnetic field B_0 and thus f_L is given by the MRI scanner in use, Q_{cc}, η and I must be matched appropriately by selecting suitable chemical compounds ('tuning').
(2) The ^{1}H must come close to the QN, as DD-coupling is proportional to $1/r^6$, r being the distance between the two nuclei. Usually, the maximum allowable distance is only a few Ångströms.
(3) The water exchange time τ_m must be fast enough so as to enrich the bulk water as much as possible with relaxed protons.

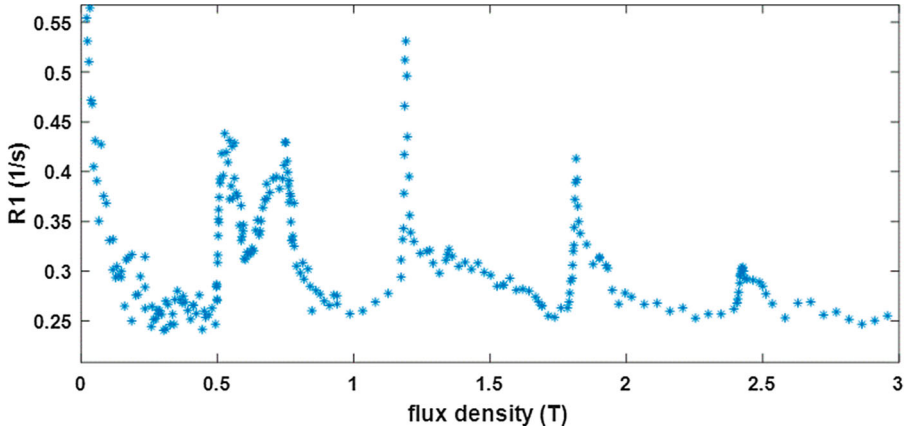

Figure 1. Example of QRE between ^{209}Bi and intrinsic protons in solid tris(2-oxymethyl-phenyl)bismuthane, see [2].

(4) The ^{1}H-QN DD coupling must fluctuate in time but not too fast because the effect gets inefficient if the rotational correlation time is too short to fulfil the condition $2\pi\nu_Q\tau_R > 1$ [4,5,10], ν_Q being the quadrupolar interaction measured in frequency units.
(5) The ensemble of QNs used in a certain moiety should have a narrow distribution of their so-called quadrupole coupling constant Q_{cc}, which reflects the product of EFG and quadrupole moment. Only in this case the transition frequencies remain within narrow limits and contribute to sharp narrow QRE peaks.

Methods for controlling condition (1) have been treated in detail in [1]. Condition 4 can be controlled by the size and form of the Bi-compounds as well as by the viscosity of the solution. When applying Stoke's formula and assuming typical viscosities for water and blood plasma one can estimate that at 3 T the hydrodynamic diameter of Bi-containing particles is required to be in the order of several nm up to several tens of nm. Therefore small molecules like the Bi-Aryl compounds investigated in [23] are too small (i.e. rotate too fast) and the rotation to be slowed down, e.g. by grafting them onto nanoparticles (NP) of suitable size and structure. Conditions 2 and 3 depend on the chemistry of the compounds and have not yet been explored in detail, but preliminary data suggest that some of the envisaged Bi-Aryl compounds allow for sufficient approach and water exchange [23].

The aim of this paper is to approach condition 5 which is particularly important to get high sensitivity of the probe to either chemical changes or B_0 field switching. This is important for instrumental design because the required B_0 changes should be kept as small as possible to avoid costly field offset inserts with high power consumption as the need for demanding mechanical and thermal management. From [23–26] one can estimate that at clinical field strengths the QRE linewidths should remain below 1 MHz, or even lower.

As a logical consequence, it is an important goal to design nanoparticles with the Bi compounds immobilised in such a way that all Bi nuclei feel essentially the same EFG. The central question is whether exclusively particles with a high degree of structural order are required or whether partially disordered structures are also suitable.

Experimentally this condition can be verified by nuclear quadrupole resonance spectroscopy (NQRS) at zero-field [6]. NQRS is essentially carried out with the same equipment as NMR, but in the absence of a static B_0 field. In this case, Zeeman splitting is absent and the pure quadrupole coupling leads to four spectral peaks in the case of a homogeneous population of spin 9/2 QNs. As described in [1] this is also a method in the process of frequency tuning (condition 1) because it allows for the determination of Q_{cc} and the so-called asymmetry parameter η. An important difference to standard NMR, however, is the need for scanning the RF frequency over very large bandwidths, usually many tens of MHz, which requires special, fast tuneable probe heads [27].

There is a vast amount of information available about NQRS in crystalline samples, either from single crystals or from crystalline powders, see, e.g. [6,7,28]. If they possess a certain molecular asymmetry and thus a non-vanishing EFG, they frequently show distinct, comparatively narrow NQR peaks. In general, crystal defects result in considerable peak broadening indicating a wider distribution of the EFG. Extremely fast T_2^* relaxation due to strong crystal defects or paramagnetic impurities [29] can lead to such excessive line broadening that the signal becomes undetectable. There are also cases where NQRS peaks cannot be observed even in high-quality crystals, i.e. in case of octahedral symmetry. Because of the sensitivity of NQRS to the EFG, the technique has been used many times for the assessment of crystallisation state [30–32]. Though crystallites provide a high degree of structural order and thus the ideal prerequisite for potentially narrow QRE peaks, they are not very useful for contrast agents. Since they have to be nano-sized, only the surface is accessible to bulk water and thus all Bi atoms in the core of the particle would not contribute to QRE. Further, the EFG at the surface is probably different between different crystal faces (different cutting planes), thus potentially broadening the resonance lines.

A reasonable alternative is thus to immobilise ensembles of Bi-Aryl molecules on or inside of biopolymeric NPs which allow for accessing water to all Bi nuclei. The question is how the immobilisation strategy affects the distribution of the EFG. Figure 2 schematically illustrates two extreme situations for two different structures. In drawing A an ensemble of Bi-molecules is embedded in a more or less disordered way, e.g. by covalent binding to a polymer. Depending on the individual local environment at each binding site, each molecule may exhibit somewhat different binding angles of the aryl-rings to the Bi atom. Therefore, each molecule experiences a slightly different EFG and the overall distribution of transition frequencies could become broad. The expected consequence would be a comparatively flat NMRD profile, as sketched below.

Drawing B, in contrast, depicts a spherical NP which offers a very regular pattern of binding sites on the surface, comparable to the periodic lattice of crystals, but in 2-D rather than in 3-D. In this case, every Bi-Aryl-compound feels more or less the same local forces and thus a strong homogeneity of the EFG is expected. As

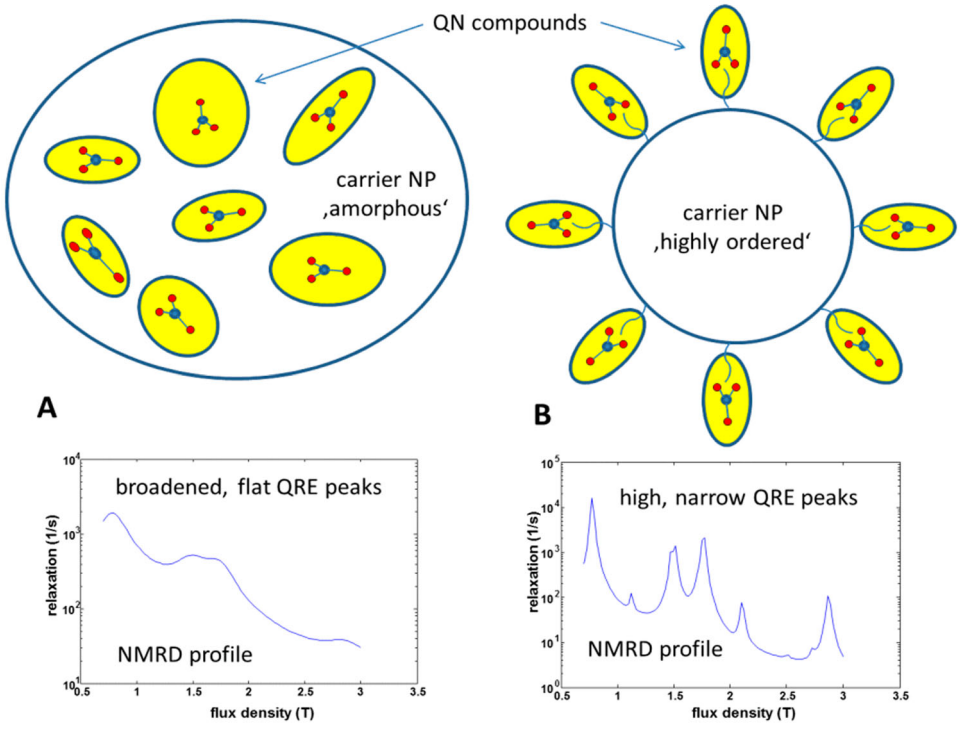

Figure 2. (A) The quadrupolar core compounds are embedded into a nano-sized carrier structure with a low degree of order. The EFG varies from site to site, symbolised by different EFG-'ellipsoids'. In case of strong EFG variation, the corresponding schematic NMRD profile is expected to have flat, broadened peaks. Panel B schematically shows a spherical carrier particle with monodisperse, homogeneous electronic surface properties providing a well-defined, repetitive electronic structure and thus a very narrow distribution of the EFG (symbolised by equal EFG-'ellipsoids') and potentially narrow, high QRE peaks.

a result, one can potentially expect narrow, high QRE peaks as sketched in the schematic NMRD profile. It should be emphasised that the NMRD curves in Figure 2 are only shown for illustration and are no real data or simulations.

The major problem is that version B, although favourable for our purposes, is more laborious to prepare. In addition, it is not known whether Bi-Aryl compounds can be embedded into the carrier matrix with a low degree of order and still preserve a narrow EFG distribution, i.e. if there exists a useful intermediate arrangement between the extreme cases A and B.

Materials and methods

To get more insight into this issue, we set up NQR experiments with two model systems comprising amorphous states of pure Triphenyl-Bismuth ($BiPh_3$). Though these are not directly representative for either type A or B because of the lack of bonding onto carrier nanoparticles, they provide an important limiting case stating the following hypothesis: If the amorphous preparations lead to considerable peak broadening then also the feasibility of useful NPs of type A is questionable. In contrast, the existence of well-detectable narrow NQR peaks would justify experiments with less rigorously structured NPs.

NQR spectroscopy

NQRS was carried out with a custom-built zero-field spectrometer as described in [27]. In order to achieve fast scanning of a wide frequency band, typical resonating NMR probe heads are not applicable because they have to be re-tuned and re-matched mechanically when changing the frequency more than the bandwidth of the resonator. Therefore custom-built probe heads were used which allow for wideband transmit without tuning and subsequent signal reception in resonator-mode with a fast electronically controllable tune/match circuit. The sample coil has an inner diameter of 5 mm so as to hold standard 5 mm NMR tubes filled with the samples. The coil sits at the end of a hollow nozzle made from teflon which can be immersed into liquid nitrogen so as to cool down the sample to 77 K which is beneficial for increasing the SNR in case of $BiPh_3$ due to an increase of the population difference between the energy levels of the QN. The used cryo-probe head operates in a frequency range of 79–116 MHz (type A4 from [27]). For cryostatisation a commercial thermos flask from stainless steel

was adapted with a special snap-lock which establishes a tight and reliable electric connection between the RF ground plane of the probe head case and the thermos flask, thus not only providing thermal insulation but also forming an excellent shield against external RF perturbations. The snap lock can be opened and closed quickly thus allowing for conveniently changing the sample tube.

All scans were carried out with a standard spin echo sequence. In case that the location of spectral peaks was not known beforehand, wideband scans were carried out with densely spaced frequency points (< 5 kHz) and using the fast interleaved sub-spectrum sampling method presented in [27]. The latter was required to keep the scanning times within reasonable limits even in the presence of the significantly prolonged T_1 time constants which typically occur at low temperatures (LN). For the scans where a high time resolution was required, the number of points was kept at 300 per spectrum and the midpoint frequency of the scanning window and the intermediate frequency filter bandwidth were set so as to capture the peaks as reliably as possible. The number of averages was chosen so as to reach the required SNR for the respective experiment, i.e. up to 2000 for the search of extremely broadened peaks with low signal and 100 for the tracking of the recrystallisation dynamics. The exact pulse settings are given in detail in the description of the individual experiments. The database for tuning and matching was re-calibrated after each change of the measurement set-up, e.g. immersion in LN or re-thawing to room temperature.

Sample preparation

Two types of experiments with different preparations of the samples were carried out.

Preparation type 1. Crystalline $BiPh_3$ powder was filled into a 5 mm NMR up to a height of 2 cm and a NQR reference spectrum was taken at room temperature (26°C = 299.15 K). Then the probe head together with the sample was immersed in LN (77 K) and another reference spectrum was acquired after a thermal equilibration interval of at least 5 min. After the scans, the samples were again thawed to room temperature.

For determination of the noise floor, a noise reference spectrum with 2000 averages was taken from an empty tube. All SNR values reported for any NQR peak in this paper were determined as the ratio between the peak amplitude and the maximum value of the noise reference spectrum. Only magnitude spectra were evaluated.

In order to form an amorphous state, the sample was molten and shock-frozen in LN. For this purpose, the probe head together with the sample was immersed in silicon oil and placed onto a prismatic Al-block with the edge lengths $10 \times 10 \times 4$ cm. The Al block was heated up with a heating plate (RCTbasic, type RCT-B, IKA Werke, Staufen, Germany). The temperature was measured continuously in the oil with a thermocouple type K connected to a multimeter MS8264, TE-Electronic. Meanwhile, the cryostat was filled with LN.

After reaching the melting temperature of 76°C the temperature was still increased by another 10–86°C so as to preserve the liquid state also for several tens of seconds after removal from the heater. Then the probe head was immediately (delay < 10 s) immersed in the LN and left in the cryostat until excessive boiling of the LN had stopped. After thermal equilibration of the sample (approx. 5 min) NQRS was started. Spectra were taken at times 0, 5, 15, 30 and 60 min after equilibration. Then the sample was withdrawn from the probe head and quickly (< 10 s) transferred to another Dewar so as to store it in LN.

For studying the NQR spectrum during the recrystallisation process the probe head was removed from the cryostat and thawed to room temperature (26°C) by immersion in a thermostatised water bath. During this procedure, a super-cooled melt formed from which recrystallisation started very quickly (within 10 min). NQR spectra were taken at the time instants 0, 3, 10, 15, 24, 60, 119 and 256 min after crystallisation. The last spectrum was taken 24 h after thawing.

The NQR pulse settings were: frequency range 75–95 MHz, echo time $T_E = 240\,\mu$s, effective repetition time $T_{Reff} = 1500\,\mu$s, IF bandwidth: 10 kHz. The pulse duration T_P was set to the optimum value for a 90° flip angle, typically 16 μs.

Preparation type 2. A 'solidified' gel with polystyrene (PS) as the matrix was produced by dissolving $BiPh_3$ in tetrahydrofurane (THF) together with PS, subsequent solvent casting and evaporation of the solvent. In that manner, a transparent clear solid with a concentration of ca. 10 wt% $BiPh_3$ was produced. This product was ground to a granulate with grain sizes < 0.5 mm and gently pressed into 5 mm NMR tubes up to a height of 2 cm with a filling factor ca 0.6.

NQRS was performed for two reference samples, i.e. crystalline $BiPh_3$ powder and the empty tube (2000 averages), respectively, as in preparation 1, and then for the granulate. All measurements were taken both at RT as well as in LN. The noise floor estimated was again estimated from the empty tube. The measurements in LN were carried out because at 77 K the signals are considerably stronger due to larger population differences between the energy levels of the QN and prolonged T_2 times.

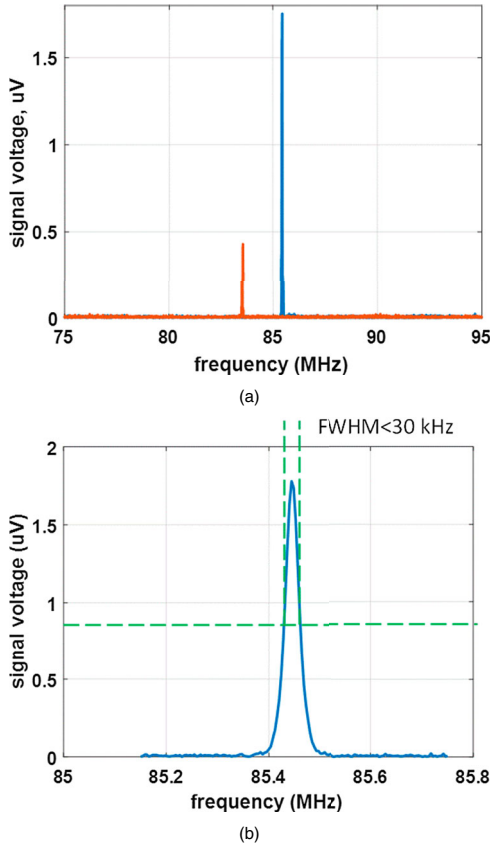

Figure 3. (A) Overlay of two NQR spectra of $BiPh_3$ between 75 and 95 MHz at RT (smaller, red peak) and at 77 K (larger, blue peak). The peaks correspond to the transition 7/2 → 5/2 of Bi and appear at 83.51 and 85.45 MHz, respectively. (B): FWHM of the peak in LN, approximately 30 kHz.

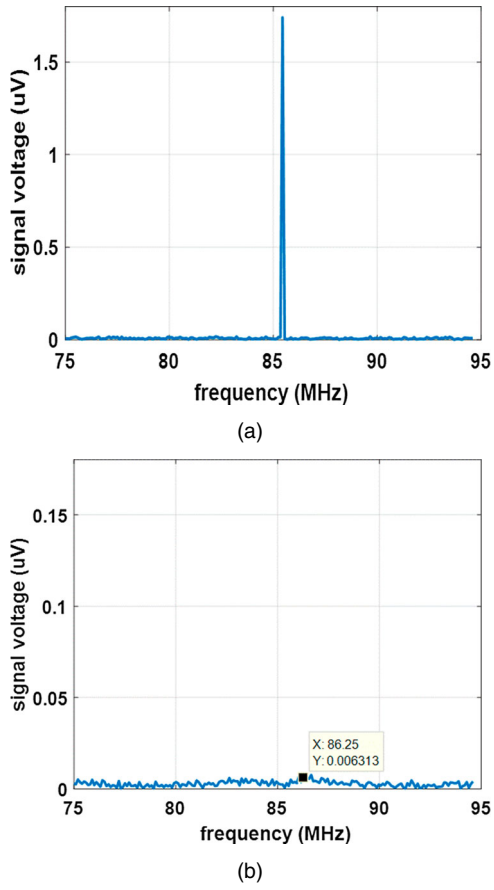

Figure 4. (A) Reference peak of crystalline powder in LN, 500 averages, peak amplitude = 1.75 µV. The SNR was approximately 300. (B) Spectrum after shock freezing of the melt (2000 averages). No peak above. $6*10^{-3}$ µV can be detected.

The exact pulse settings were: frequency range 75–95 MHz, $T_{\mathrm{Reff}} = 2000\,\mu$s, IF bandwidth: 10 kHz, $T_{\mathrm{P}} = 16\,\mu$s. The echo time was chosen as low as possible, here $T_{\mathrm{E}} = 80\,\mu$s, in order to account for potential T_2 shortening.

Results

Figure 3(A) shows an example of two overlayed wideband spectra of crystalline $BiPh_3$ powder in a band between 75 and 95 MHz. One can clearly identify the strong peak of the transition 7/2 → 5/2 of the nuclear spin both at RT as well as at 77 K. The respective peak frequencies occur at 83.5 and 85.45 MHz, respectively. As expected the peak amplitude is by a factor of nearly 4 greater at 77 K than at RT due to the larger population difference at low temperature according to the underlying Boltzmann-distribution, see, e.g. [33]. The full width at half maximum (FWHM) of the peak at 77 K was approximately 30 kHz (Figure 3(B)) while the amplitude was 1.75 µV. All peak frequencies were in perfect agreement with previously published data [34].

NQRS in preparation 1

After shock freezing in LN, no peak above noise level could be detected anymore in the whole frequency span of the probe head.

When regarding Figure 4(B) hardly any peak can be observed with an amplitude > 0.006 µV. At this signal level ringdown artefacts of the probe head start dominating the signal, thus the apparent features in the graph are most likely spurious and should not be interpreted anymore. Therefore, at the detection limit we find an amplitude reduction by at least 290. Assuming the conservation of the overall signal power (still all Bi nuclei produce a signal, but it is dispersed over a wide frequency range) and conservation of the T_1 and T_2 relaxation times this would mean a broadening by the same factor. With the original bandwidth being 30 kHz we can thus state that the peak has been broadened to more than 8.7 MHz in case that the T_1 and T_2 time constants have remained constant.

After thawing to room temperature $BiPh_3$ formed a super-cooled melt (liquid state) from which

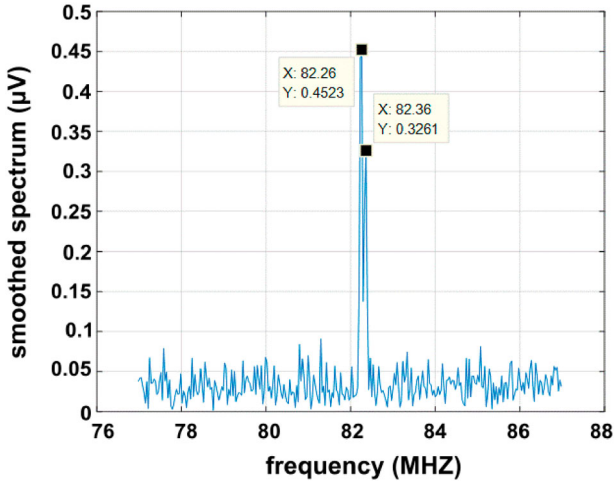

(a)

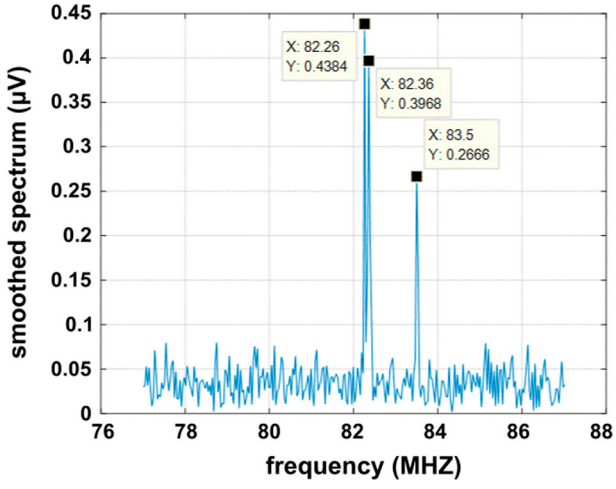

(b)

Figure 5. (A) NQR spectrum at RT, immediately after re-crystallisation. A double peak has appeared at 82.26 MHz and 82.39 MHz, respectively. (B): NQR spectrum 70 min after re-crystallisation. A smaller peak at the original location (83.51 MHz) has appeared.

re-crystallisation started within a few minutes. Ten minutes after thawing the melt had entirely crystallised, yielding a coarsely grained white product.

Interestingly instead of the peak at 83.5 MHz the NQR spectrum of this product showed a clear double peak at 82.26 MHz and 82.36 MHz MHz as shown in Figure 5(A). Fifteen minutes afterwards a small peak at the original frequency of 83.5 MHz had appeared the amplitude of which increased steadily with progressing time, while the double peak slowly decreased. The state after 70 min is shown in Figure 5(B). After 24 h the double peak had disappeared completely, while the original peak at 83.51 MHz was completely re-established. In synchrony with this process the coarsely grained first crystallisation product was continuously converted into a fine powder from top to bottom of the tube, forming a sharp border

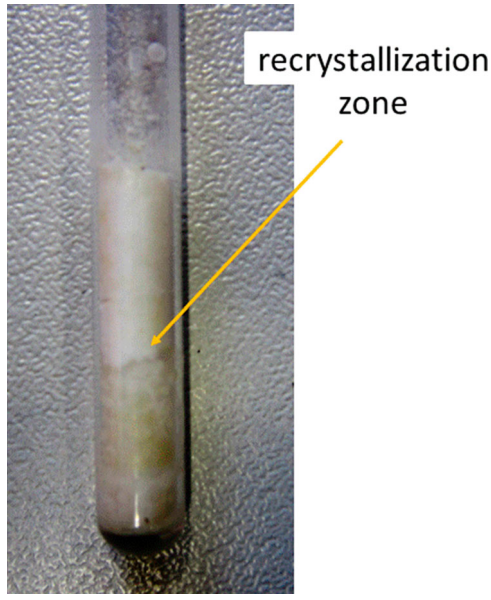

Figure 6. Photograph of the sample during the re-crystallisation of $BiPh_3$ from the metastable phase to the stable original phase (after ca 2 h). One can clearly see the border between the upper, stable powder and the lower, metastable phase. The black zone at the bottom of the tube is a colour artefact due to poor illumination.

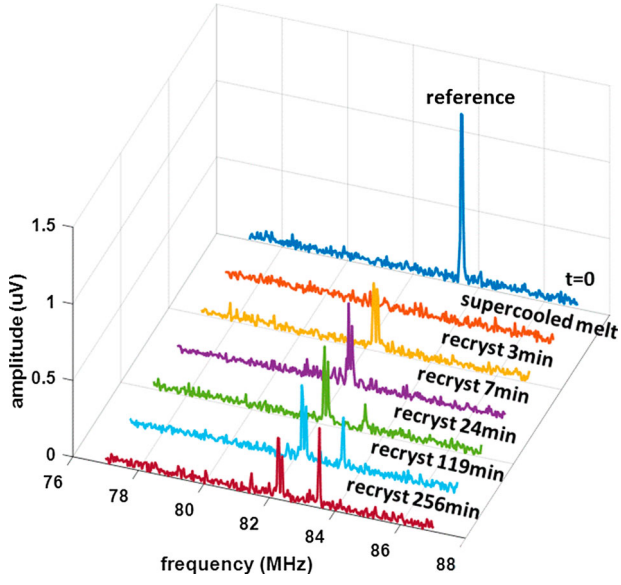

Figure 7. Evolution of the NQR spectrum during recrystallisation of $BiPh_3$ from a super-cooled melt after thawing from the amorphous state at 77 K to RT. The large peak in the uppermost trace is the reference peak before shock freezing, to which the sample had entirely returned after approximately 24 h. Spectra at 3 and 7 min after the start of crystallisation show the double peak of the metastable phase. The latest three spectra show the re-growth of the original peak of the stable $BiPh_3$ powder at the simultaneous decrease of the metastable double peak. It should be emphasised that for scaling reasons the grid is not equidistant in time.

between the two phases which slowly moved downward, see Figure 6. Obviously, the double peak was associated with the first metastable crystallisation product while the final fine powder represented the stable standard form of $BiPh_3$.

Figure 7 shows the evolution of the NQR spectrum during the recrystallisation process in form of a 3-D plot with seven selected time points. It should be emphasised, however, that the time axis is not equidistantly scaled because the plot would be stretched in a very unfavourable way which would severely hamper its readability.

NQRS in preparation 2

The solidified PE gel (10% $BiPh_3$) did not yield any detectable peak, neither when measured in LN nor at RT. As the detection limit was fairly the same as in preparation 1, i.e. 0.00 5μV, a 10% crystalline phase with filling factor 0.6 would have been expected to yield a narrow peak similar to Figure 4(A) with an amplitude of 0.105 μV, i.e an SNR of 21. With the same reasoning as in preparation 1 the gel peak has thus been broadened to a FWHM $>$ 630 kHz, if we again assume no change of the relaxation time constants T_1 and T_2.

Discussion

Experiments involving NQR spectroscopy with two solid preparations of triphenyl-bismuth have shown, that the sharp resonance peaks of pure quadrupole transitions disappear if the crystalline structure of the solids is destroyed, i.e. if they are transformed into an amorphous state. This happens, e.g. when shock-freezing molten compounds in liquid nitrogen (preparation 1) or dissolving the powders in a mixture of PS and THF and subsequent solidification by evaporating the solvent (preparation 2). In both cases, it is assumed that the peaks have been broadened so significantly that they have dropped below the limit of detectability.

Of course, it should be kept in mind that we have assumed the relaxation time constants to remain in the range which is required for reliable detection. This, of course, is not self-evident because we do not know how the destruction of the crystalline states affects these parameters. There is, of course, a probability that dynamics of the molecules in the amorphous form changes and, although the signal remains detectable, it is considerably modulated by different relaxation properties of the system. In case of a drop of T_2 below 20 μs the detection of a peak becomes very difficult because the echo time of one spin echo cannot be reasonably decreased below 50 μs with our probe heads and pulse powers. However, such short values would be more than one order of magnitude lower than those published for crystalline BiPh3, i.e. $T_2 = 802$ 16,400 ed that the extreme broadening is caused by a broad distribution of the EFG which occurs when passing to the amorphous states. For preparation 1 this hypothesis is quite probable because the EFG depends very sensitively on the binding angles of the chemical bonds between Bi and the Phenyl rings. Shock freezing the molecules from a melt, where the binding angles are subject to vibrational fluctuations could easily lead to a state with a broad distribution of instantaneous 'snapshots' of different phases of these vibrations [35]. The disappearance of the NQR peak is thus not very surprising. In the solid gel, however, the situation is different because the solidification by evaporation is a slow process and leaves enough room for the molecules to attain their energetically most probable configuration, which then would not exclude a narrow distribution. Nevertheless, we found a significant peak broadening which raises the question whether the EFG, in fact, depends on the individual neighbourhood of the single molecules to the PS chains. As we can expect a low degree of order in such gels we further conclude that structural order has high importance for narrow EFG distributions.

As a side product of our investigations we also observed the formation of a metastable crystal phase during the re-crystallisation of the amorphous BiPh3. In all repetitions of the experiments a super-cooled melt formed at room temperature after thawing the shock-frozen product. The observation of the NQR peaks at 82.26 MHz and 82.39 MHz suggests a new crystal phase which, however, is quickly and spontaneously converted to the regular phase of $BiPh_3$ at RT. The experiment primarily served for confirming that the passage to and from the amorphous state is reversible, but so far we have not conducted additional experiments to characterise the phase transitions, because this was not the focus of our investigations. We do also not have information on the crystal structure of the metastable phase because the latter is extremely sensitive and spontaneously returns to the stable state when mechanically manipulating the sample, e.g. when cutting the tube for removal. There is thus the need for further refined experiments involving, e.g. continuous SAXS during the recrystallisation process, for further characterising the metastable phase.

Conclusion

Our experimental data suggest that amorphous states can significantly broaden the distribution of the EFG in Bi-triaryl compounds and consequently also the peaks of NQR as well as QRE. In the context of designing sensitive responsive nanoprobes for MRI, we thus conclude that condition (5) for efficient QRE is closely linked to

the structural order of the core molecules. In this case, appropriate nanoparticles which serve as carriers should preferentially have a highly ordered, crystal-like structure so that all quadrupolar compounds on or within them feel essentially the same EFG.

Acknowledgement

The authors would also like to acknowlegde the COST Action CA15209, supported by COST (European Cooperation in Science and Technology) which stimulated relevant personal communications with several NMR relaxometry experts.

Disclosure statement

No potential conflict of interest was reported by the authors.

Funding

This project has received funding from the European Union's Horizon 2020 research and innovation programme (FET-open) under grant agreement No. 665172.

ORCID

Christian Gösweiner http://orcid.org/0000-0003-4453-9385
Stefan Spirk http://orcid.org/0000-0002-9220-3440
Danuta Kruk http://orcid.org/0000-0003-3083-9395

References

[1] C. Gösweiner, P. Lantto, R. Fischer, C. Sampl, E. Umut, P.-O. Westlund, D. Kruk, M. Bödenler, S. Spirk, A. Petrovič and H. Scharfetter, Phys. Rev. X. **8**, 021076 (2018).
[2] D. Kruk, E. Umut, E. Masiewicz, C. Sampl, R. Fischer, S. Spirk, C. Goesweiner and H. Scharfetter, Phys. Chem. Chem. Phys. PCCP. **20**, 12710 (2018).
[3] D. Kruk, *Understanding Spin Dynamics* CRC Press, New York, 2015.
[4] P.-O. Westlund, Phys. Chem. Chem. Phys. PCCP. **12**, 3136 (2010).
[5] P.-O. Westlund, Mol. Phys. **110**, 2251 (2012).
[6] T.P. Das, E.L. Hahn, *Solid State Physics: Supplement 1: Nuclear Quadrupole Resonance Spectroscopy*, 1st ed., Academic Press Inc., New York, 1958.
[7] B.H. Suits, *Handbook of Applied Solid State Spectroscopy* edited by D.R. Vij, Springer, Boston, 2006, 6596.
[8] M. Florek-Wojciechowska, M. Wojciechowski, R. Jakubas, S. Brym and D. Kruk, J. Chem. Phys. **144**, 054501 (2016).
[9] W. Masierak, M. Florek-Wojciechowska, I. Oglodek, R. Jakubas, A.F. Privalov, B. Kresse, F. Fujara and D. Kruk, J. Chem. Phys. **142**, 204503 (2015).
[10] D. Kruk, A. Kubica, W. Masierak, A.F. Privalov, M. Wojciechowski and W. Medycki, Solid State Nucl. Magn. Reson. **40**, 114 (2011).
[11] D. Kruk, F. Fujara, P. Gumann, W. Medycki, A.F. Privalov, C. Tacke and S.S. Nucl, Magn. Reson. **35**, 152 (2009).
[12] É. Tóth, L. Helm, and A.E. Merbach, in *Contrast Agents I* (Springer, Berlin, Heidelberg, 2002), pp. 61–101.
[13] P. Caravan, Chem. Soc. Rev. **35**, 512 (2006).
[14] I. Bertini, C. Luchinat and G. Parigi, Adv. Inorg. Chem. **57**, 105 (2005).
[15] A.S. Merbach, L. Helm, É Tóth, *The Chemistry of Contrast Agents in Medical Magnetic Resonance Imaging* John Wiley & Sons, Chichester, 2013.
[16] J. Kowalewski, D. Kruk and G. Parigi, Adv Inorg Chem **57**, 41 (2005).
[17] F. Winter and R. Kimmich, Biophys. J. **48**, 331 (1985).
[18] R. Kimmich, W. Nusser and F. Winter, Phys Med Biol **29**, 593 (1984).
[19] D.J. Lurie, G.R. Davies, M.A. Foster and J.M.S. Hutchison, Magn Reson Imaging. **23**, 175 (2005).
[20] D.J. Lurie, S. Aime, S. Baroni, N.A. Booth, L.M. Broche, C.H. Choi, R. Davies, S. Ismail, DÓ hÓgáin and K.J. Pine, Comptes Rendus Phys. **11**, 136 (2010).
[21] Y. Fujiwara, M. Mitani, S. Yasuike, J. Kurita and T. Kaji, J. Health Sci. **51**, 333 (2005).
[22] P.C. Naha, A.A. Zaki, E. Hecht, M. Chorny, P. Chhour, E. Blankemeyer, D.M. Yates, W.R.T. Witschey, H.I. Litt, A. Tsourkas and D.P. Cormode, J. Mater. Chem. B Mater. Biol. Med. **2**, 8239 (2014).
[23] H. Scharfetter, C. Gösweiner, E. Umut, C. Sampl, R. Fischer, S. Spirk, A. Petrovic and D. Kruk, Proc Intl Soc Mag Reson Med. **20** (2018).
[24] M. Bödenler, M. Basini, M.F. Casula, E. Umut, C. Gösweiner, A. Petrovic, D. Kruk, H. Scharfetter, J. Magn Reson. 1997 **290**, 68 (2018).
[25] C.T. Harris, W.B. Handler, Y. Araya, F. Martínez-Santiesteban, J.K. Alford, B. Dalrymple, F.V. Sas, B.A. Chronik and T.J. Scholl, Magn. Reson. Med. **72**, 1182 (n.d.).
[26] L. de Rochefort, E. Lee, M. Polello, L. Durrasse, G. Ferrante and B.K. Rutt, Proc Intl Soc Mag Reson Med. **20** (2012).
[27] H. Scharfetter, M. Bödenler and D. Narnhofer, J. Magn. Reson. **286**, 148 (2018).
[28] M. Bloom, E.L. Hahn and B. Herzog, Phys. Rev. **97**, 1699 (1955).
[29] L.A. Zemnukhova, S.I. Kuznetsov and R.L. Davidovich, Russ. Chem. Bull. **47**, 2169 (1998).
[30] S.C. Pérez, M. Zuriaga, P. Serra, A. Wolfenson, P. Negrier and J.L. Tamarit, J. Chem. Phys. **143**, 134502 (2015).
[31] I.N. Pen'kov and I.A. Sofin, Int Geol Rev **9**, 793 (1967).
[32] T.J. Bastow, J.A. Lehmann-Horn and D.G. Miljak, Solid State Nucl. Magn. Reson. **71**, 55 (2015).
[33] M.H. Levitt, *Spin Dynamics: Basics of Nuclear Magnetic Resonance*, 2nd ed. (Wiley, Chichester, 2008).
[34] H. Chihara and N. Nakamura, in *Nucl. Zr - Bi*, edited by K.-H. Hellwege and A.M. Hellwege (Springer-Verlag, Berlin/Heidelberg, 1989), pp. 230–243.
[35] R.J.F. Berger, D. Rettenwander, S. Spirk, C. Wolf, M. Patzschke, M. Ertl, U. Monkowius and N.W. Mitzel, Phys. Chem. Chem. Phys. **14**, 15520 (2012).